J. Chem. Sci. (2020) 132:89
https://doi.org/10.1007/s12039-020-01799-w

REGULAR ARTICLE

A ninhydrin–thiosemicarbazone based highly selective and sensitive chromogenic sensor for Hg^{2+} and F^- ions

V RAJU[a,b], R SELVA KUMAR[a], S K ASHOK KUMAR[a,*], G MADHU[b], SHILPA BOTHRA[c] and SUBAN K SAHOO[c]

[a]Department of Chemistry, School of Advanced Sciences, Vellore Institute of Technology, Vellore 63 2014, India
[b]Center for Applied Science, Sree Vidyanikethan Engineering College, Tirupati 517 102, India
[c]Department of Applied Chemistry, SV National Institute Technology, Surat 395 007, India
E-mail: ashok312002@gmail.com

MS received 25 March 2020; revised 4 May 2020; accepted 14 May 2020

Abstract. This study demonstrates the design, synthesis and sensing applications of a simple and efficient chemosensor, 2-(1,3-dioxo-1H-inden-2(3H)-ylidene)hydrazinecarbothioamide (**R**) for quick detection of Hg^{2+} and F^- in aqueous media using a colorimetric test, UV–Vis spectral analysis, and silica gel support. Sensor **R** showed the typical absorption peak at 305 nm for Hg^{2+} which is responsible for color change from yellow to colorless, while in the case of F^-, **R** exhibits a major peak at 415 nm and a color change from yellow to red. The limit of detection (LOD) of **R** for the analysis of Hg^{2+} was calculated as 1×10^{-6} M while for F^-, it was found to be 3.4×10^{-7} M. The binding modes of **R** with Hg^{2+} and F^- have been investigated by the Job's plot, Benesi–Hildebrand (BH) method, ^{1}H NMR, FTIR and theoretical studies. The sensor **R** was reversible after treating it with reagents such as EDTA and calcium nitrate solution after contacting with Hg^{2+} and F^-, respectively. The performance of **R** can be successfully applied for the analysis of F^- contents present in toothpastes.

Keywords. Chemosensor; colorimetry; mercury; fluoride; density functional theory.

1. Introduction

The design and development of optical sensors for selective and sensitive monitoring of heavy-transition metal ions and biologically important anions have attracted much attention in supramolecular chemistry over the past few decades.[1–7] In particular, the recognition and sensing of extremely dangerous and toxic Hg^{2+} and F^- ions are very significant in biological and environmental systems.[8–13] Hg^{2+} is one of the most toxic heavy metal, affecting the human health and ecosystem, and it can bioaccumulate throughout the food chain as hazardous methyl mercury species (CH_3Hg). An overexposure of Hg^{2+} leads to various ill effects with neurological damages, such as prenatal brain damage, cognitive and motion disorders and Minamata disaster.[14, 15] Apart from this, it can also form useful amalgams with various metals, which find numerous applications in diverse fields.

Fluoride ions play a vital role in a wide range of biological, medical and chemical processes, such as dental caries, osteoporosis treatment, anesthetic and even in chemical warfare agents.[16–20] Besides these, intense levels of fluoride in drinking water can lead to severe health disorders, including dental and skeletal fluorosis, and osteosarcoma, also cause nephrotoxic changes and urolithiasis in humans.[21–23] Numerous approaches have been reported till date, but they suffer from several drawbacks such as difficulty in synthesis, poor sensitivity in organic phase detection, and use of highly sophisticated instruments. Therefore, an extremely sensitive and selective analytical method is required for the determination of Hg^{2+} and F^-. However, several fluorometric, colorimetric chemosensors as well as chemodosimeters were reported for the

*For correspondence

Electronic supplementary material: The online version of this article (https://doi.org/10.1007/s12039-020-01799-w) contains supplementary material, which is available to authorized users.

Published online: 01 August 2020

detection of Hg^{2+} as well as fluoride based on chemical bond formation,[24] hydrogen bonding,[25] complexation[26] and organometallic compound formation. A few chemosensors are capable of sensing Hg^{2+} and F^- in partial aqueous media and limited reports are for 100% aqueous medium. Hence, a chemosensor competent of highly selective colorimetric sensing of Hg^{2+} and F^- can be extremely advantageous, particularly for use in an aqueous environment.

Thiosemicarbazones are considered as a potent structural moiety which are used in many biologically active compounds,[27] and these analogues are popular for their pharmacological significance, particularly as antiparasitic, antibacterial and antitumor agents.[28] These derivatives act as ligands and can also act as complexing agents for metal ions[29] and anions[30] due to the presence of versatile binding sites. As a continuation of our study on the development of ligands for cations and anions recognition,[31] herein we report, the synthesis and sensing properties of a new ninhydrin thiosemicarbazone (**R**) as a colorimetric sensor for recognition of Hg^{2+} and F^- in an aqueous environment.

2. Experimental

2.1 *Materials and methods*

All solvents used are of HPLC grade and used without any further purification. Ninhydrin, thiosemicarbazide, metal chlorides and anions (sodium salt) were used in the purest form. All spectroscopic experiments were carried out at room temperature. ^{1}H NMR spectra were recorded on a Bruker AM 400 spectrometer with tetramethylsilane (TMS) as an internal reference and DMSO-d_6 as solvent. FTIR spectra of the samples were recorded on Nicolet AVATAR 380 FTIR spectrophotometer using the potassium bromide (KBr) pellet method. The pH was measured using Eutech pH–510 meter.

The working solutions of metal salts and sodium salt anions were prepared in double-distilled water for analysis with the ligand **R**. For UV–Visible spectral studies, the metal ions K^+, Mg^{2+}, Al^{3+}, Pb^{2+}, Ni^{2+}, Cr^{3+}, Co^{2+}, Mn^{2+}, Cu^{2+}, Zn^{2+}, $Hg^{2+,}$ and Fe^{3+} were added as their chlorides and anions F^-, Cl^-, Br^-, I^-, OH^-, $H_2PO_4^-$, CH_3COO^- as their sodium salts respectively. For selectivity study, 1 mL of cations or anions (5×10^{-4} M) was added in 5 mL vials containing **R** (1 mL, 1×10^{-5} M). The spectra were recorded for each sample on a JASCO V-730 spectrophotometer wavelength range 200–800 nm with a quartz cuvette of 1 cm path length.

2.2 *Synthesis of R*

The ligand **R** was prepared in a single-step condensation reaction of ninhydrin with thiosemicarbazide in water medium as shown in Scheme 1. A mixture of compounds of ninhydrin (1.78 g, 1 mM) and thiosemicarbazide (0.911 g, 1 mM) in 20 mL of water was subjected to reflux for 10 min. After completion of the reaction, a brownish solid was separated by filtration. The final product was treated with cold ethanol and re-crystallized with absolute ethanol. The purified **R** was characterized by NMR (^{1}H ^{13}C), FTIR and HR-MS.

The characteristics of **R** are as follows: yield (92%), color (brownish), melting point of the compound 178–180°C. FTIR spectra (cm^{-1}): 3448 (N–H, 2° amine); 2994, 2912 (N–H, 1° amine); 2104 (N=N–); 1655 (C=N); 1406 (C=O); 1310, 1018, 950 (C=S) (-Figure 1S, Supplementary Information). ^{1}H NMR (DMSO-d_6, ppm): 6.94 (s, H, NH_2), 7.36 (s, H, NH_2), 7.62-7.92 (m, 4H, Ar-H), 9.98 (s, H, NH) (Figure 2S, Supplementary Information). ^{13}C (DMSO-d_6, ppm): 87.49, 90.37, 123.44, 125.19, 130.54, 132.41, 136.70, 150.25, 178.77, 194.24 (Figure 3S, Supplementary Information). HR-MS (ESI) m/z calculated for $C_{10}H_7N_3O_2S$ $[M+H]^+$: 233.0293, found: 233.1431 (Figure 4S, Supplementary Information).

3. Results and Discussion

3.1 *Recognition of Hg^{2+} and F^- ions*

The chromogenic sensing performance of **R** towards diverse metal ions was studied in the presence and absence of different metal ions, such as K^+, Mg^{2+}, Al^{3+}, Pb^{2+}, Ni^{2+}, Cr^{3+}, Co^{2+}, Cu^{2+}, Mn^{2+}, Hg^{2+}, Zn^{2+} and Fe^{3+} in aqueous media by the naked-eye color change and recording the corresponding UV–Vis spectra. The ligand **R** showed a distinct color change from yellow to colorless upon interaction of Hg^{2+} as shown in Figure 1a. Under identical environment, no such noticeable color changes were observed in the presence of other tested metal ions (K^+, Mg^{2+}, Al^{3+}, Pb^{2+}, Ni^{2+}, Cr^{3+}, Co^{2+}, Cu^{2+}, Mn^{2+}, Zn^{2+} and Fe^{3+}). Similarly, the sensing ability of **R** towards various

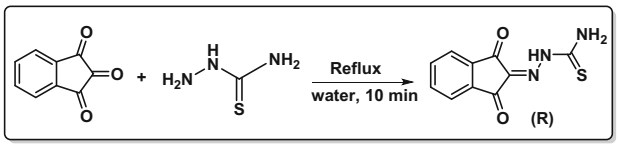

Scheme 1. Reagents and conditions to synthesize **R**.

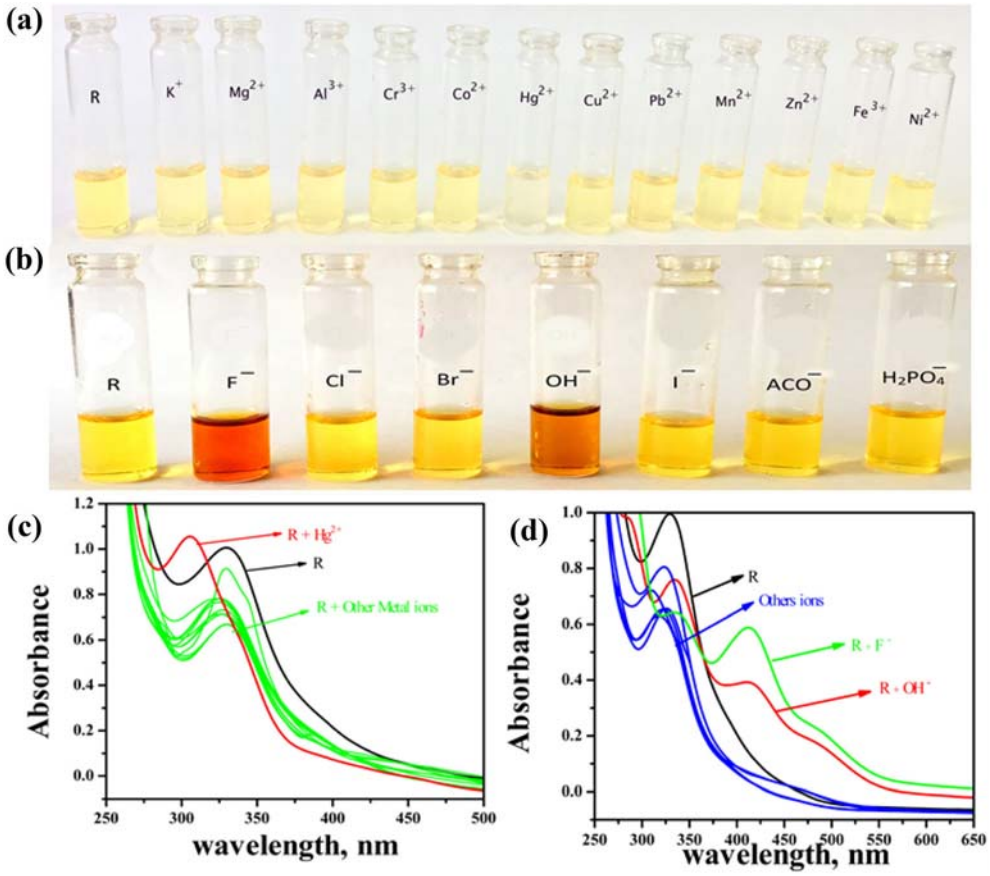

Figure 1. Colorimetric and UV–Visible spectral performance of **R** (20 μM) with various selected analyte (2 mM): metal ions (a, c) and anions (b, d).

anions like F^-, Cl^-, Br^-, I^-, OH^-, $H_2PO_4^-$ and CH_3COO^- were also investigated in aqueous media. **R** showed a fabulous color change from yellow to red upon the addition of F^- as shown in Figure 1b. Further, the UV–Visible absorption spectra of **R** in the absence and presence of tested metal ions and anions were recorded and the results are shown in Figure 1, c&d. The ligand **R** exhibits a major absorption band at 335 nm, which may be due to ligand-to-ligand charge transitions (LLCT). Upon the addition of Hg^{2+}, the most noteworthy changes resulted were an instantaneous appearance of a new blue-shifted absorption band at 305 nm and this peak shift was due to the change of the ligand to metal ion charge transition upon complexation. This new peak was accountable for the change of color from yellow to colorless, which was perceptible to the naked eye. Further, **R** showed almost no spectral changes upon the addition of K^+, Mg^{2+}, Al^{3+}, Pb^{2+}, Ni^{2+}, Cr^{3+}, Co^{2+}, Cu^{2+}, Mn^{2+}, Zn^{2+} and Fe^{3+} which discriminated Hg^{2+} from the other tested metal ions. Similarly, the interaction of F^- with **R** resulted in the instantaneous appearance of the new red-shifted absorption band at 415 nm in the visible region. This was due to the interaction of imine hydrogen with highly electronegative F^- species and correspondingly forms a hydrogen bond and subsequently, proton departs from **R** and undergoes an extensive charge transfer leading to red shift. The binding affinity between **R** and Hg^{2+} along with the sensitivity of ligand **R** was recognized by conducting UV–Visible titration. The sequential addition of Hg^{2+} in aqueous solution was added to **R**. As the titration proceeded, the λ_{max} of **R** at 335 nm shifted to 305 nm (Figure 2a) due to the formation of **R–Hg^{2+}**. The limit of detection (LOD) of **R** as a sensor for the recognition of Hg^{2+} was calculated from the calibration curve by applying the IUPAC guidelines: LOD=3σ/slope (where 'σ' denotes the standard deviation of the blank sample) and it was calculated down to 1×10^{-6} M (Figure 3a). The obtained LOD was compared with the recently reported Hg^{2+} selective chemosensors. Similarly, the sensitivity of **R** towards F^- was analyzed by UV–Visible titration on successive addition of F^- to **R**, which exhibited a distinct new red-shifted absorption band at 415 nm in the visible region and showed three isosbestic points (375 nm, 310 nm and 280 nm) as a result of the formation of new complex species (Figure 2b). This

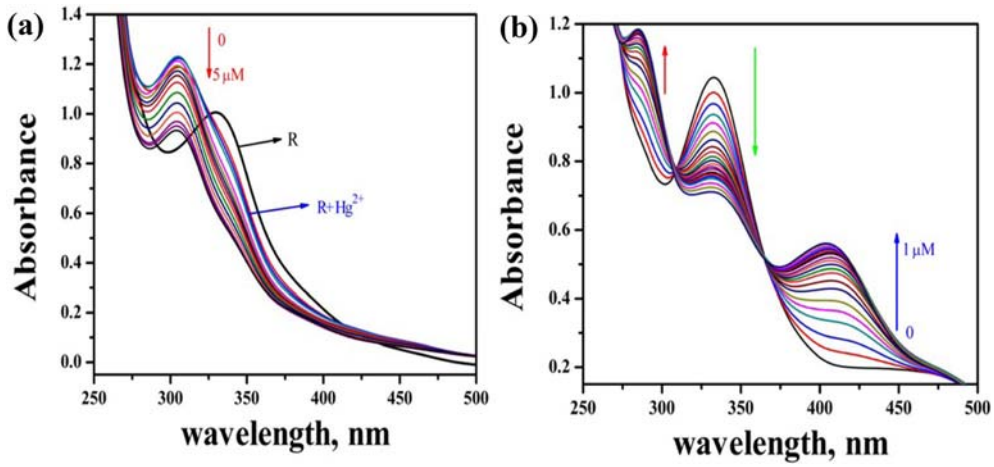

Figure 2. (a) UV–Visible spectral changes of **R** (2×10^{-5} M) in aqueous media after the addition of Hg^{2+} (0–5 μM), (b) F^- (0–1 μM).

behavior is due to the deprotonation of –NH proton on the interaction of F^- and subsequently, the excess electrons present on amide nitrogen undergoes extensive delocalization. The calculated LOD of F^- was found to be 3.4×10^{-7} M (Figure 3b). Also, the absorption band of **R** with the addition of different concentrations of F^- was found to obey Beer's law by showing a linear response at 415 nm.

3.2 *Effect of pH*

Further, the effect of pH on the absorbance of complexes (**R–Hg^{2+}** and **R–F$^-$**) was studied in the pH range of 2.0–12.0. It has been found that the absorbance and wavelength maximum of **R–Hg^{2+}** and **R–F$^-$** complex remained unchanged over the pH variation of 6.0–9.0 and 7.0–9.0 respectively. Beyond this pH range of the complexes (**R–Hg^{2+}** and **R–F$^-$**), the visual color and absorbance changes occurred due to deprotonation of amide nitrogen in the basic region and protonation in the acidic region. In case of **R–Hg^{2+}** complex, formation of $Hg(OH)_2$ takes place in in basic region while in acid region protonation leads to decrease in absorbance while in case of **R–F$^-$**, in the basic region due to increase in OH^- concentration, further enhancement in absorbance intensity was noticed, but in the acid region, due to protonation absorbance intensity was decreased. Hence, the working pH range for Hg^{2+} and F^- determination were found to be 6.0–9.0 and 7.0–9.0 respectively (Figure 4, a&b).

3.3 *Binding constant, stoichiometry, reversible and competitive studies*

The binding constant (K_a) was calculated using the BH method by plotting the change in absorbance against the concentration of analyte $1/[Hg^{2+}]$ or $1/[F^-]$

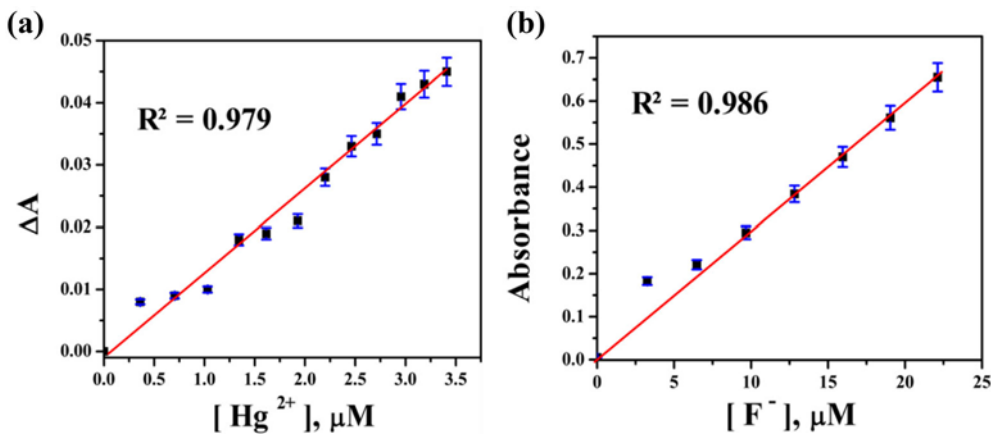

Figure 3. Calibration plot of **R** with (a) Hg^{2+} and (b) F^-.

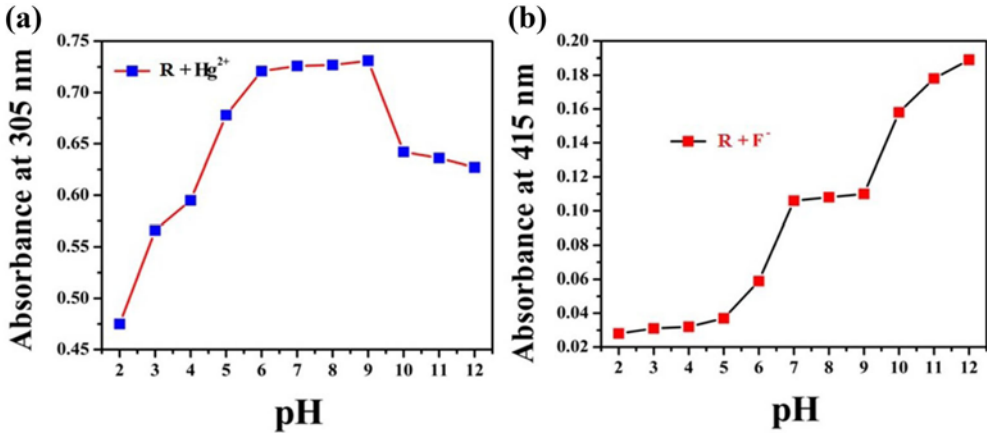

Figure 4. Effect of pH on (a) **R–Hg^{2+}** and (b) **R–F^{-}**.

(Figure 5, a&b). The magnitude of K_a is estimated from the calibration curve and the binding constant for **R** with Hg^{2+} and F^{-} was found to be 3.3×10^4 M^{-1} and 4.6×10^4 M^{-1}, respectively. Further, the binding stoichiometry of **R** with Hg^{2+} and F^{-} was performed individually using Job's method. The obtained results show that the formation of 1:1 ligand to metal/anion ratio (Figure 5, c&d). To ensure the reversible response of the ligand-to-metal ion interaction, the binding reversibility of the **R–Hg^{2+}** complex in aqueous media was investigated. Owing to the high stability constant of EDTA–Hg^{2+} complex, it was expected that EDTA will complex with Hg^{2+} from the **R–Hg^{2+}** complex. As shown in Figure 6a, the absorbance of the **R–Hg^{2+}** complex was diminished upon interaction with EDTA (2 equiv.). Further, the

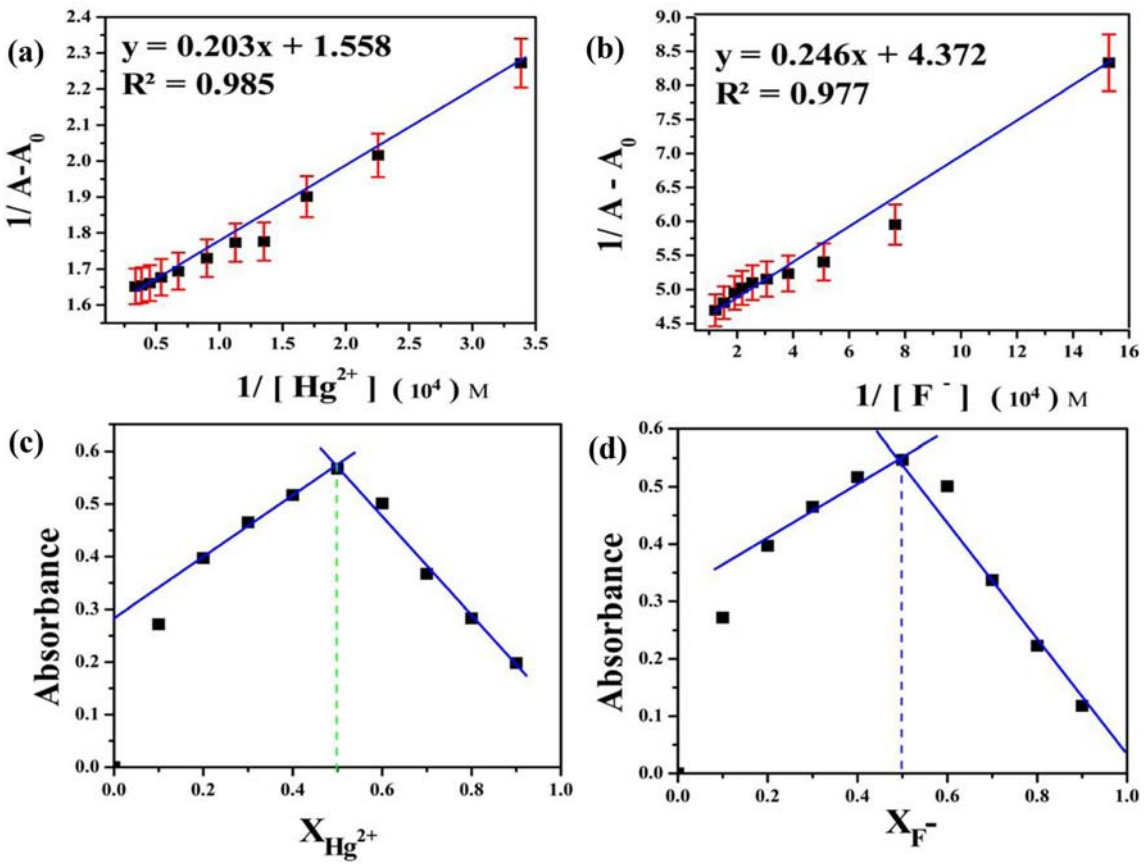

Figure 5. BH and Job's plot of **R** with Hg^{2+} (a, c) and F^{-} (b, d).

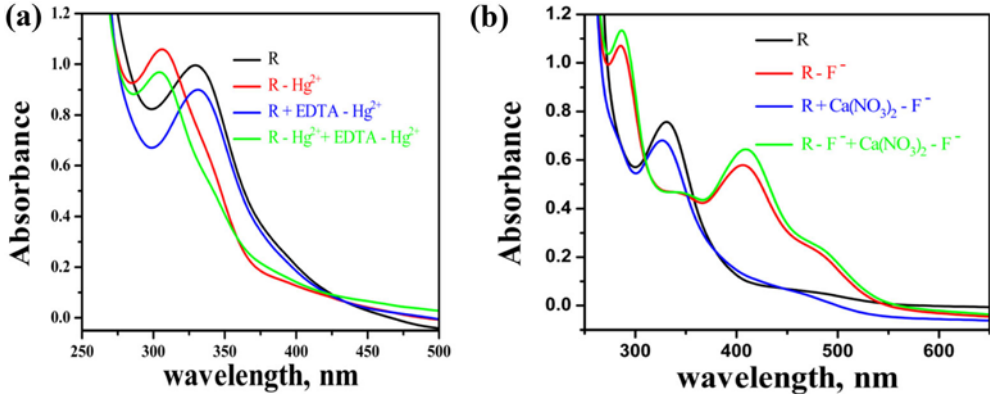

Figure 6. Reversible changes of **R** (20 μM) with (a) Hg^{2+} and EDTA (b) F^- and $Ca(NO_3)_2$.

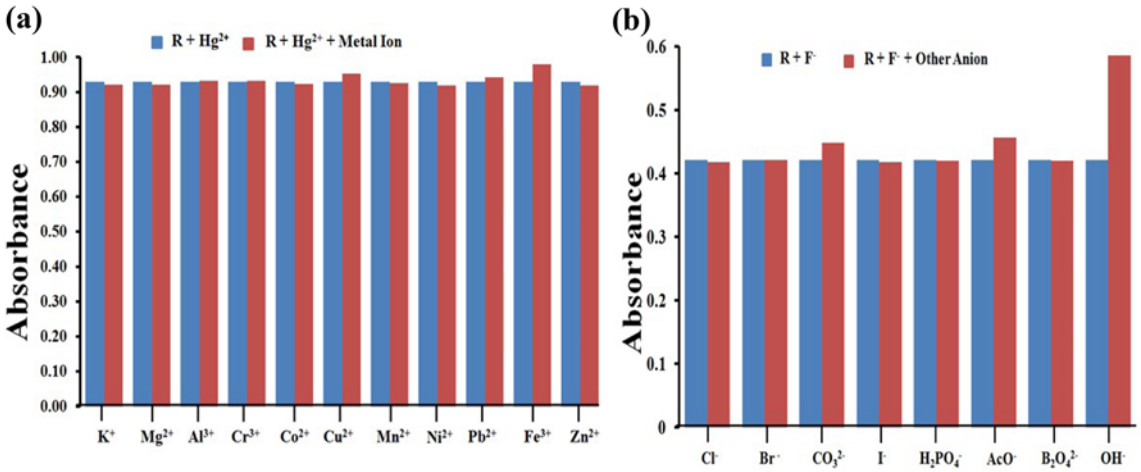

Figure 7. Selectivity performance of **R** towards (a) Hg^{2+} in the presence of other metal ions. (b) F^- in the presence of other anions.

accumulation of Hg^{2+} resulted in the recovery of spectral response, signifying the binding of **R** with Hg^{2+} is chemically reversible. Likewise, the binding reversibility of F^- to **R** in aqueous media is also conducted. Due to the high formation constant for CaF_2, it was expected that Ca^{2+} will combine with F^- from **R–F**$^-$ complex. The absorbance of the **R–F**$^-$ complex diminished upon the addition of calcium nitrate (Figure 6b). Further, the addition of F^- resulted in the recovery of spectral response representing the binding of ligand **R** with F^- is reversible.

To further investigate the utility of **R** as a Hg^{2+} selective chromogenic sensor, competitive experiments were conducted by the use of binary metal ion systems under similar circumstances (Figure 7a). The obtained results of the detection of Hg^{2+} was not substantially perturbed by the background of other coexisting species, such as K^+, Mg^{2+}, Al^{3+}, Pb^{2+}, Ni^{2+}, Cr^{3+}, Co^{2+}, Cu^{2+}, Mn^{2+}, Zn^{2+}, and Fe^{3+} ions. Yet there exhibits a small change in absorption maxima in the presence of coexisting species, but it shows excellent selectivity of the chemosensor for Hg^{2+} in aqueous media. Similarly, to investigate the selectivity of **R** towards F^- over other coexisting species, such as Cl^-, Br^-, $H_2PO_4^-$, I^-, AcO^-, CO_3^{2-}, $B_2O_4^{2-}$ and OH^- ions, competitive experiments were conducted. In the presence of other tested anions, it failed to demonstrate any noteworthy alteration in the photophysical behavior (Figure 7b), except in the presence of OH^-.

To authenticate the real-time recognition of cations and anions, the response time of **R** in the existence of Hg^{2+} and F^- ions were investigated. The obtained result reveals that the binding interaction between

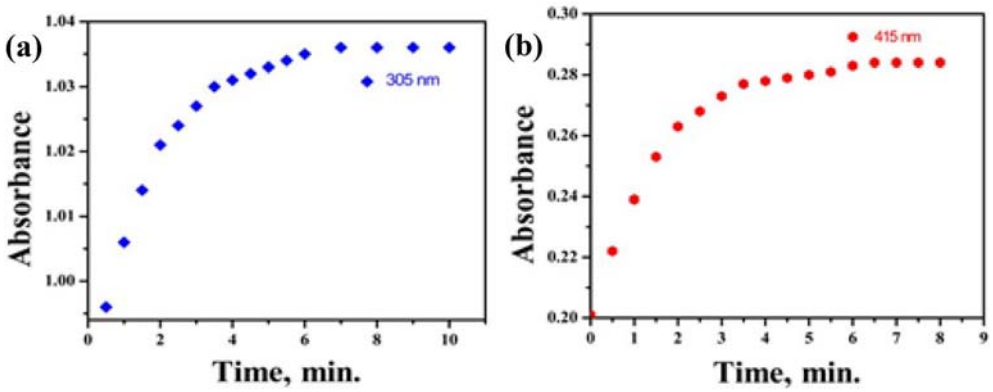

Figure 8. Time evolution study of **R** in the presence (a) Hg^{2+} and (b) F^{-}.

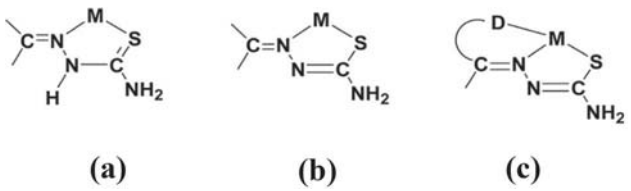

Scheme 2. Possible interaction modes of thiosemicarbazones.

R and Hg^{2+} ions continued until 4th min (Figure 8a) while the binding of **R** with F^{-} almost completed within 2 min (Figure 8b). Owing to the geometrical complementarity combined with the weak hydrogen bond interaction, the binding of **R-F^{-}** involved a short response time and there is a strong hydrogen bond interaction as well as delocalization of ligand, which would have been the probable reason for the longer response time required for the detection process.

3.4 *Binding studies*

The different binding modes of thiosemicarbazones with metal ions are represented in three different ways; neutral thione form (**A**) or in the anionic thiolate form (**B**) as bidentate NS donor ligands forming five-membered chelate rings.[32, 33] The binding capacity of thiosemicarbazones is further enhanced by condensation of thiosemicarbazide with an aldehyde or ketone consisting of an additional donor atom (D) in a suitable position for complexation, resulting in tri-coordination (**C**) (Scheme 2).[34–36]

To investigate the qualitative bonding ability of ligand **R** with Hg^{2+} and F^{-}, FTIR spectral titration was carried out. The FTIR spectra of ligand **R** were recorded in the presence and absence of these ions individually. The free **R** showed peaks at 3300–3500 cm^{-1} for secondary amine, >N–H stretch for NH_2 as a doublet occurs at 2994–2912 cm^{-1}, N=N– bond vibrates at 2104 cm^{-1}, C=O and C=N occur at 1655 cm^{-1} and 1406 cm^{-1} respectively. The thiocarbonyl group resonates at 951 cm^{-1}, 1018 cm^{-1} and 1309 cm^{-1}, respectively. When the ligand **R** interacts with Hg^{2+}, major changes were seen in the peak positions and intensity at 1655 cm^{-1}, 1406 cm^{-1}, 1018 cm^{-1}, and 3300–3500 cm^{-1}. The variations at 1655 cm^{-1}, 1406 cm^{-1} and 1018 cm^{-1} explain the interaction of C=O, C=N, C=S functional groups with Hg^{2+}.

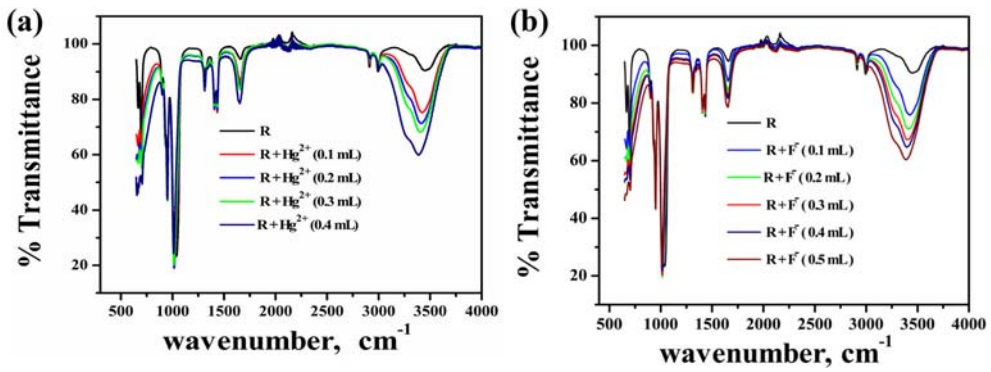

Figure 9. FTIR spectral titration (a) **R–Hg^{2+}** and (b) **R–F^{-}**.

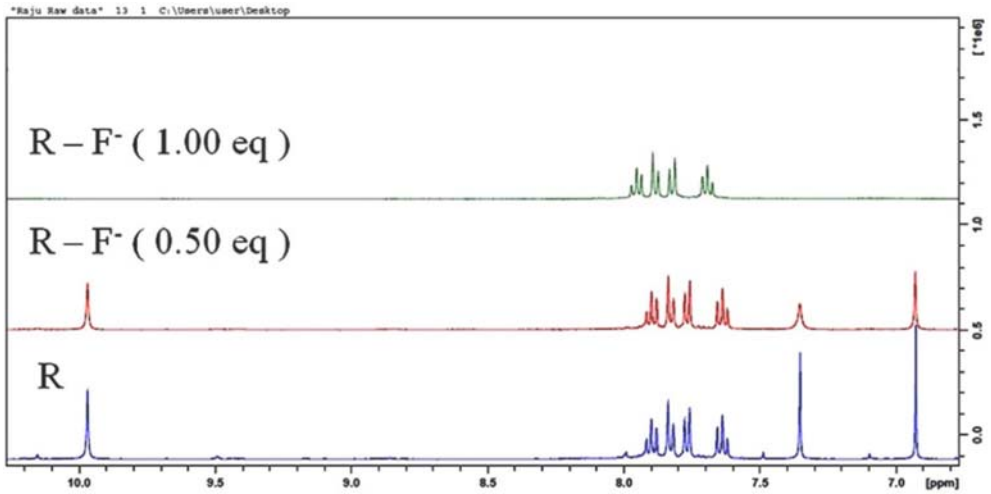

Figure 10. ^{1}H NMR titration of **R** with F^{-}.

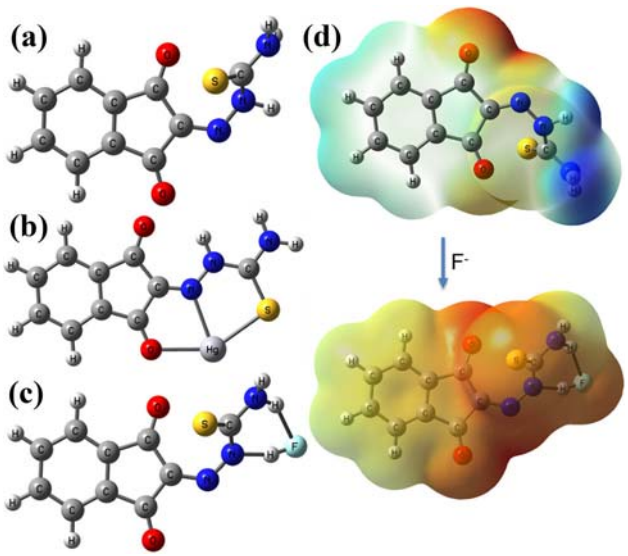

Figure 11. DFT computed optimized structure of (a) **R** and its complex with, (b) Hg^{2+}, (c) F^{-}, (d) the molecular electrostatic potential (MEP) map of **R** and its complex with F^{-}.

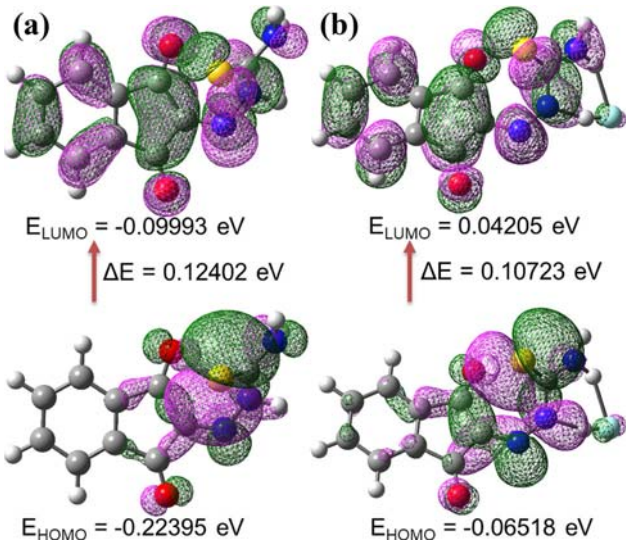

Figure 12. The computed LUMO and HOMO diagrams of (a) **R** and its (b) **R**$-$**F**$^{-}$ complex.

Figure 13. Practical application of **R** for the detection of Hg^{2+} and F^{-} by silica support method where A: R (20 mM), B: Hg^{2+}/F^{-} (20 mM), C: Hg^{2+}/F^{-} (2×10^{-2} M).

However, the modifications observed at 3300–3500 cm^{-1} were due to the interaction of water molecules with >N–H unit. Further, when **R** interacts with F^{-}, major changes were observed at 3300–3500 cm^{-1} due to H-bonding formation with F^{-} ions. As the concentration of F^{-} increased, spectral changes were observed at 1655 cm^{-1}, 1406 cm^{-1}, and 1018 cm^{-1}. This may be due to the intramolecular charge transfer, as shown in Figure 9, a&b.

^{1}H NMR titration was carried out to establish the binding mode of **R** with F^{-} in DMSO-d_6 (Figure 10). The free **R** exhibits four different peaks at 10 ppm, 7–8 ppm, 7.35 ppm and 6.9 ppm were due to the presence of NH, aromatic protons and NH_2 protons. On sequential addition of F^{-}, the intensity of the N–H (thiourea) signal at 10 ppm diminishes. This indicates that the deprotonation of N–H is involved, thereby the

electron density present on nitrogen atom experiences resonance results in the de-shielding effect on aromatic protons. However, both NH_2 protons also disappear due to liable protons.

Considering the experimental evidence, the 3D structure of the **R** and its complexes with Hg^{2+} and F^- were obtained by applying the density functional theory (DFT) method in the gas phase. All calculations were performed using the exchange-correlation functional B3LYP and the basis sets LANL2DZ for Hg atom, whereas 6-31G** for the remaining F, C, H, N and O atoms coded in the computational program Gaussian 09W.[37] The computed structures are shown in Figure 11. The ligand **R** provided a suitable tridentate coordination site to coordinate Hg^{2+} ion, which resulted in the lowering of the interaction energy ($E_{int} = E_{complex} - E_{ligand} - 2E_{Hg2+/F-}$) by −240.16 kcal/mol. The bond lengths for the Hg–S, Hg–O, and Hg–N bonds were respectively obtained as 2.608, 2.378 and 2.455 Å. The anionic analyte F^- interacted with **R** with the protons of the groups –NH– and $–NH_2$ through the hydrogen bonding. The two binding sites can be defined from the computed molecular electrostatic potential map (MEP), where the most positive region was observed over the groups –NH– and $–NH_2$ (Figure 11d) highlighted in blue color. After getting the ground state geometry optimization, the interaction energy (E_{int}) was found to be lowered by −108.09 kcal/mol upon complexation of **R** with F^-, which indicates a strong affinity between the ligand **R** and F^-. Also, the bond lengths of the groups –NH– and $–NH_2$ increased upon interaction with F^-. The most significant increase in the bond length was observed in the –NH– group from 1.015 Å to 1.535 Å, which supported the deprotonation mechanism proposed from the experimental evidence.

Further, the lowest unoccupied molecular orbital (LUMO) and the highest occupied molecular orbital (HOMO) of the **R** and **R–F**$^-$ complex were analyzed (Figure 12). Due to the elongation of the –NH– bond in **R** upon interaction with F^-, the charge delocalization increases due to increased conjugation, and the HOMO energy was increased from −0.22395 eV to −0.06518 eV. Also, comparing the distribution of HOMO and LUMO charge density along with the MEP of **R–F**$^-$ (Figure 11d) supported the intramolecular charge transfer (ICT) occurred between F^- ions and the ligand **R**. As a consequence, the energy gap between the HOMO and LUMO of **R** was reduced from 0.12402 eV to 0.10723 eV upon complexation with F^- that accords well with the red-shift in the absorption spectra of **R** towards visible region, observed experimentally.

3.5 *Applications*

Further, the qualitative recognition of Hg^{2+} by **R** was worked on a solid support. The silica gel (60–120 mesh, 10 g, colorless) was first treated with **R** in methanol (20 mL, 10^{-2} M), and then dried to get a significantly faint yellow color silica gel loaded with **R** on the surface. When the silica-loaded **R** was contacted with 1 mL of Hg^{2+} (1×10^{-2}, 1×10^{-3} M), significant color changes of the silica gel were observed and are shown in Figure 13. A similar procedure was adopted for F^-, and a considerable color change of the silica gel-loaded **R** was observed. Also, the analytical feature of the present sensor was used for the determination of Hg^{2+} and F^- contents in different water systems and toothpaste samples (Figures 5S and 6S, Supplementary Information). All analysis was obtained from triplicate measurements with the **R** sensor and results were in satisfactory agreement with those determined by recovered values as seen from the Table 1S (Supplementary Information). Besides, the performance of the ligand **R** has been compared and summarized in Table 2S (Supplementary Information) with reported work.[38–47] It concludes that the present ligand is good in terms of sensitivity, response time, wide working pH range and has good water tolerance, and ligand can be prepared via simple synthetic route.

4. Conclusion

In conclusion, we demonstrated a highly selective and sensitive colorimetric chemosensor for remarkable sensing of Hg^{2+} and F^- ions using **R** as the ligand. The ligand **R** selectively displayed a naked-eye detectable color change from yellow to colorless and red, concerning Hg^{2+} and F^- ions respectively. The synthesis of **R** is easy as compared to the ligand reported in the literature, and this ligand can find potential applications in various samples for the accurate estimation of Hg^{2+} and F^- ions.

Supplementary Information (SI)

Supplementary information associated with this article is available at www.ias.ac.in/chemsci.

Acknowledgements

Authors are grateful to the Department of Science and Technology, GOI for supporting the work through the project grant (EMR/2017/000816). Authors are also thankful to DST-VIT-FIST for NMR and GC-MS for research facilities.

References

1. Aragay G, Pons J and Merkoçi A 2011 Recent trends in macro-, micro-, and nanomaterial-based tools and strategies for heavy-metal detection *Chem. Rev.* **111** 3433
2. Carter K P, Young A M and Palmer A E 2014 Fluorescent sensors for measuring metal ions in living systems *Chem. Rev.* **114** 4564
3. Cho D G and Sessler J L 2009 Modern reaction-based indicator systems *Chem. Soc. Rev.* **38** 1647
4. Kaur K, Saini R, Kumar A, Luxami V, Kaur N, Singh P and Kumar S 2012 Chemodosimeters: an approach for detection and estimation of biologically and medically relevant metal ions, anions and thiols *Coord. Chem. Rev.* **256** 1992
5. Santos-Figueroa L E, Moragues M E, Climent E, Agostini A, Martínez-Máñez R and Sancenon F 2013 Chromogenic and fluorogenic chemosensors and reagents for anions. A comprehensive review of the years 2010–2011 *Chem. Soc. Rev.* **42** 3489
6. Sareen D, Kaur P and Singh K 2014 Strategies in detection of metal ions using dyes *Coord. Chem. Rev*. **265** 125
7. Xu Z, Chen X, Kim H N and Yoon J 2010 Sensors for the optical detection of cyanide ion *Chem. Soc. Rev.* **39** 127
8. Formica M, Fusi V, Giorgi L and Micheloni M 2012 New fluorescent chemosensors for metal ions in solution *Coord. Chem. Rev.* **256** 170
9. Gai L, Mack J, Lu H, Nyokong T, Li Z, Kobayashi N and Shen Z 2012 Organosilicon compounds as fluorescent chemosensors for fluoride anion recognition *Coord. Chem. Rev.* **285** 24
10. Kim H N, Ren W X, Kim J S and Yoon J 2012 Fluorescent and colorimetric sensors for detection of lead, cadmium, and mercury ions *Chem. Soc. Rev.* **41** 3210
11. Nolan E M and Lippard S J 2008 Tools and tactics for the optical detection of mercuric ion *Chem. Rev.* **108** 3443
12. Yang Y, Zhao Q, Feng W and Li F 2012 Luminescent chemodosimeters for bioimaging *Chem. Rev.* **113** 192
13. Zhou Y, Zhang J F and Yoon J 2014 Fluorescence and colorimetric chemosensors for fluoride-ion detection *Chem. Rev.* **114** 5511
14. Ayoob S and Gupta A K 2006 Fluoride in drinking water: a review on the status and stress effects *Crit. Rev. Environ. Sci. Technol.* **36** 433
15. Cametti M and Rissanen K 1983 Recognition and sensing of fluoride anion *Chem. Commun.* **20** 2809
16. Wergedal J E and Baylink D J Fluoride directly stimulates proliferation and alkaline phosphatase activity of bone-forming cells *Science* **222** 330
17. Kleerekoper M The role of fluoride in the prevention of osteoporosis *Endocrinol. Metab. Clin*. **27** 441
18. Yamaguchi S, Akiyama S and Tamao K Colorimetric fluoride ion sensing by boron-containing π-electron systems *J. Am. Chem. Soc.* **123** 11372
19. Cittanova M L, Lelongt B, Verpont M C, Geniteau-Legendre M, Wahbe F, Prie D, Coriat P and Ronco P M 1996 Fluoride ion toxicity in human kidney collecting duct cells *Anesthesiology* **84** 428
20. Kim S Y, Park J, Koh M, Park S B and Hong J I 2009 Fluorescent probe for detection of fluoride in water and bioimaging in A549 human lung carcinoma cells *Chem. Commun.* **31** 4735
21. Singh P, Barjatiya M, Dhing S, Bhatnagar R, Kothari S and Dhar V 2001 Evidence suggesting that high intake of fluoride provokes nephrolithiasis in tribal populations *Urol. Res.* **29** 238
22. Wang C and Wong K M C 2013 Selective Hg^{2+} sensing behaviors of rhodamine derivatives with extended conjugation based on two successive ring-opening processes *Inorg. Chem.* **52** 13432
23. He S, Liu Q, Li Y, Wei F, Cai S, Lu Y and Zeng X 2014 Rhodamine 6G-based chemosensor for the visual detection of Cu^{2+} and fluorescent detection of Hg^{2+} in water *Chem. Res. Chinese Univ.* **30** 32
24. Khatua S and Schmittel M 2013 A single molecular light-up sensor for quantification of Hg^{2+} and Ag^{+} in aqueous medium: high selectivity toward Hg^{2+} over Ag^{+} in a mixture *Org. Lett.* **15** 4422
25. Parthiban C, Manivannan R and Elango K P 2015 Highly selective colorimetric sensing of Hg (II) ions in aqueous medium and in the solid state via formation of a novel M–C bond *Dalt. Trans.* **44** 3259
26. Varghese A and George L 2012 Simultaneous first order derivative spectrophotometric determination of vanadium and zirconium in alloy steels and minerals *Spectrochim. Acta Part A Mol. Biomol. Spectrosc.* **95** 46
27. Easmon J, Pürstinger G, Heinisch G, Roth T, Fiebig H H, Holzer W, Jäger W, Jenny M and Hofmann J 2001 Synthesis, cytotoxicity, and antitumor activity of copper (II) and iron (II) complexes of 4 N-azabicyclo[3.2.2]nonane thiosemicarbazones derived from acyl diazines *J. Med. Chem.* **44** 2164
28. Chellan P, Nasser S, Vivas L, Chibale K and Smith G S 2010 Cyclopalladated complexes containing tridentate thiosemicarbazone ligands of biological significance: Synthesis, structure and antimalarial activity *J. Organomet. Chem.* **695** 2225
29. Calatayud D G, López Torres E and Mendiola M A 2013 A fluorescent dissymmetric thiosemicarbazone ligand containing a hydrazonequinoline arm and its complexes with cadmium and mercury *Eur. J. Inorg. Chem.* **1** 80
30. Su H, Huang W, Yang Z, Lin H and Lin H 2012 2-Hydroxy-naphth-1-aldehyde phenyl-thiosemicarbazone: effective thiourea-based sensor for acetate anion *J. Incl. Phenom. Macrocycl. Chem.* **72** 221
31. Raju V, Ashok Kumar S K, Abbareddy D S, Rao M and Sahoo S K 2017 Isatin-3-phenylhydrazone: a highly selective colorimetric chemosensor for copper, chromium and cobalt ions in semi-aqueous medium *Sens. Lett.* **15** 266
32. West D X, Liberta A E, Padhye S B, Chikate R C, Sonawane P B, Kumbhar A S and Yerande R G 1993 Thiosemicarbazone complexes of copper(II): structural and biological studies, *Coord. Chem. Rev.* **123** 49
33. Tian Y P, Duan C Y, Lu Z L, You X Z, Fun H K and Kandasamy S 1996 Crystal structure and spectroscopic studies on metal complexes containing ns donor ligands derived from S-benzyldithiocarbazate and p-dimethylaminobenzaldehyde *Polyhedron.* **15** 2263

34. Souza P, Matesanz A I and Fernández V 1996 Copper (II) and cobalt (II) complexes of methyl 2-pyridyl ketone thiosemicarbazone (HL); single-crystal structure of [Cu (HL) L] NCS *J. Chem. Soc. Dalt. Trans.* **14** 3011
35. Lu Z, White C, Rheingold A L and Crabtree R H 1993 Deprotonated thioamides as thiolate S-donor ligands with a high tendency to avoid MSM bridge formation: crystal and molecular structure of bis(2-hydroxy-5-methylacetophenone N,N-dimethylthiosemicarbazonato)dinickel *Inorg. Chem.* **32** 3991
36. Kumar R R, Ramesh R and Małecki J G 2016 Steric control on the coordination behaviour of carbazole thiosemicarbazones towards [RuH (Cl)(CO)(AsPh 3)3]: a combined experimental and theoretical study *New J. Chem.* **40** 10084
37. Frisch M J *et al*. 2009 Gaussian 09, Revision A.02 (Wallingford, CT: Gaussian, Inc.)
38. Wu C, Wang J, Shen J, Bi C and Zhou H 2017 Coumarin-based Hg^{2+} fluorescent probe: Synthesis and turn-on fluorescence detection in neat aqueous solution *Sensors Actuators B Chem.* **243** 678
39. Wang J, Li W and Long L 2017 Development of a near-infrared fluorescence turn-on probe for imaging Hg^{2+} in living cells and animals *Sensors Actuators B Chem.* **245** 462
40. Guo Z, Zhu W, Zhu M, Wu X and Tian H 2010 Near infrared cell permeable Hg^{2+} selective ratiometric fluorescent chemodosimeters and fast indicator paper for $MeHg^{+}$ based on tricarbocyanines *Chem. Eur. J.* **16** 14424
41. Momidi B K, Tekuri V and Trivedi D R 2016 Selective detection of mercury ions using benzothiazole based colorimetric chemosensor *Inorg. Chem. Commun.* **74** 1
42. Pan J T, Zhu F, Kong L, Yang L M, Tao X T, Tian Y P, Lu H B and Yang J X 2015 A simple pyridine-based colorimetric chemosensor for highly sensitive and selective mercury (II) detection with the naked eye *Chem. Pap.* **69** 527.
43. Ma L, Leng T, Wang K, Wang C, Shen Y and Zhu W 2017 A coumarin-based fluorescent and colorimetric chemosensor for rapid detection of fluoride ion *Tetrahedron* **73** 1306
44. Chavali R, Gunda N S K, Naicker S and Mitra S K 2015 Rapid detection of fluoride in potable water using a novel fluorogenic compound 7-O-tert-butyldiphenylsilyl-4-methylcoumarin *Anal. Chem. Res.* **6** 26
45. Mohammadi A and Jabbari J 2016 Simple naked-eye colorimetric chemosensors based on Schiff-base for selective sensing of cyanide and fluoride ions *Can. J. Chem.* **94** 631
46. Chen Z J, Wang L M, Zou G, Zhang L, Zhang G J, Cai X F and Teng M S 2012 Colorimetric and ratiometric fluorescent chemosensor for fluoride ion based on perylene diimide derivatives *Dye. Pigment.* **94** 410
47. Vinithra G, Suganya S and Velmathi S 2013 Naked eye sensing of anions using thiourea based chemosensors with real time application *Tetrahedron Lett.* **54** 5612